# Quantum Teleportation under Non-Hermitian Operations

Yangchen Wu,[1] Huangqiuchen Wang,[1] Zihao Li,[1] Yihao Kang,[1] Bo Liu,[2,*] Lijiong Shen,[1,†] and Zhe Sun[1,‡]

[1] *School of Physics, Hangzhou Normal University, Hangzhou 310036, China*
[2] *School of Information and Electrical Engineering, Hangzhou City University, Hangzhou, 310015, China*

We investigate the standard quantum teleportation protocol for a single-qubit state, focusing on the scenario where the qubit undergoes a class of non-unitary evolution governed by parity-time ($\mathcal{PT}$)-symmetric non-Hermitian Hamiltonians. Additionally, we examine the case where the entangled pair shared by Alice and Bob is exposed to a noisy channel. In the $\mathcal{PT}$-symmetric regime, the teleportation fidelity exhibits time-dependent oscillations. Compared to the conventional case without non-Hermitian operations, periodic enhancements in fidelity are observed, and we analytically derive their dependence on the parameters of both the non-Hermitian Hamiltonian and noisy channel. When the $\mathcal{PT}$ symmetry is broken, the fidelity ceases to oscillate and instead decays to a steady value. Notably, even in this regime, non-Hermitian operations can yield fidelity improvements over conventional schemes. We further investigate the teleportation of quantum Fisher information (QFI) and find that its evolutionary behavior differs from that of fidelity. Analytical results reveal that QFIs corresponding to different estimated parameters exhibit distinct outcomes at Bob's receiving end during teleportation. Furthermore, we derive a trade-off inequality between fidelity and QFI, offering a theoretical tool to coordinately optimize these two quantities in the teleportation process.

## I. INTRODUCTION

Quantum teleportation [1], a cornerstone of quantum information science, leverages quantum entanglement [2] and classical communication to transmit quantum state information between spatially separated systems. This process enables the reconstruction of the original quantum state in the receiver without physically transferring the quantum system [3–9]. It underpins critical applications in quantum computing, communication, and cryptography [10–13]. However, environmental noise poses significant challenges to its practical implementation [14–16]. Such noise disrupts the stability of the entanglement and reduces the efficiency of quantum operations, thereby diminishing the fidelity of transmitted quantum states [17–19]. Theoretical models [20] and experimental studies [21] demonstrate that phase-damping noise, for instance, causes an exponential decay of teleportation fidelity with increasing distance. Noise channels fundamentally determine the range of transmittable quantum states [20], particularly providing the well-documented noise-dependent robustness of the entanglement held by the qubits in quantum teleportation [22].

To mitigate these effects, conventional strategies such as quantum error correction [23] and entanglement distillation [24] are commonly employed. However, these approaches often require substantial quantum resources and involve complex operations [25]. For instance, surface-code-based error correction can achieve logical error rates on the order of $10^{-4}$ [26], but at the cost of quadratic resource overhead with increasing code distance [27]. To address the challenges of quantum decoherence in open quantum systems, non-Hermitian systems [28, 29] have gained considerable attention due to their distinctive physical properties. Theoretical and experimental studies demonstrate that non-Hermitian operations enhance the robustness of entanglement distribution in quantum communication protocols by precisely controlling the evolution of entangled states [30]. Moreover, non-Hermitian systems offer significant potential for improving measurement precision, thereby advancing quantum sensing and parameter estimation techniques [31–33]. A special class of non-Hermitian systems exhibiting $\mathcal{PT}$ symmetry can be characterized by real eigenvalue spectra and predictable quantum evolution, whereas $\mathcal{PT}$-symmetry-breaking cases feature complex eigenvalues and nontrivial dynamics [34]. Therefore, fundamentally distinct dynamical behaviors emerge between the $\mathcal{PT}$-symmetric and $\mathcal{PT}$-symmetric-breaking regimes [35–39].

Building upon the unique advantages of non-Hermitian quantum operations, our research aims to uncover their potential to enhance teleportation performance in noisy channels. In this study, we conduct a systematic analysis across three canonical noise channels: phase-damping, amplitude-damping, and bit-flip channels. We employ a dual-metric framework, utilizing both fidelity (to quantify state transfer accuracy) and quantum Fisher information (QFI, to assess parameter estimation precision) [40] to comprehensively characterize quantum information transfer in a non-Hermitian quantum teleportation protocol. Remarkably, in the $\mathcal{PT}$-symmetric regime, periodic enhancements of the teleportation fidelity and teleported QFI can be found. Through analytical derivation, we identify the enhancement time regions, which exhibit dependence on the parameters of non-Hermitian operations, noisy channels and input states. Notably, different noise channels manifest distinct widths of enhance-

* liuboheqingbo@126.com
† shenlijiong@hznu.edu.cn
‡ sunzhe@hznu.edu.cn

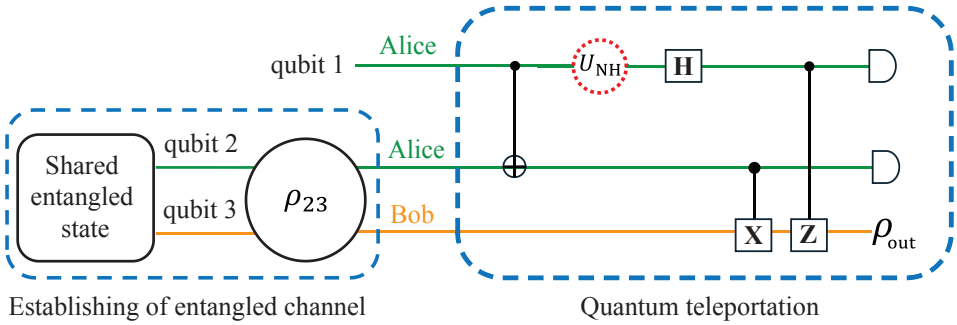


Figure 1. Quantum teleportation circuit under a non-Hermitian operation. The sender, Alice, holds a quantum state $|\psi_{\rm in}\rangle$ (Eq. 1) on qubit 1 to be teleported. Alice and the receiver, Bob, share a maximally entangled state on qubits 2 and 3. Alice applies a CNOT gate, with qubit 1 as the control and qubit 2 as the target, entangling qubit 1 with qubit 2 through an entanglement swap. She then applies the non-Hermitian Hamiltonian followed by a Hadamard gate on qubit 1. Alice performs projective measurements on the bases of qubits 1 and 2, and sends the measurement results to Bob via a classical communication channel. Based on the received classical bits, Bob applies the corresponding unitary operation on qubit 3, reconstructing Alice's initial quantum state.

ment windows. We further examine the differences and connections between the teleportation fidelity and teleported QFI, ultimately establishing a trade-off inequality relation between these metrics. This theoretical framework provides novel insights into quantum information transmission during a non-Hermitian quantum teleportation in noisy environments.

The paper is organized as follows: in Sec. II, we introduce the theoretical framework of quantum teleportation under non-Hermitian operations. In Sec. III, we systematically analyze the fidelity dynamics, examining both $\mathcal{PT}$-symmetric and $\mathcal{PT}$-symmetry-breaking operations across three decoherence channels: phase-damping (Sec. III A), amplitude-damping (Sec. III B), and bit-flip channel (Sec. III C). In Sec. IV, we investigate the teleported QFI of parameter $\phi$ (Sec. IV A)and the teloported QFI of parameter $\theta$ (Sec. IV B) in $\mathcal{PT}$-symmetric and $\mathcal{PT}$-symmetry-breaking regimes. In Sec. IV C, we establish the relationship between fidelity and QFI. Finally, we conclude our work in Sec. V.

## II. QUANTUM TELEPORTATION UNDER NON-HERMITIAN OPERATOR

As illustrated in Fig. 1, Alice possesses a quantum state to be teleported, which is encoded on qubit 1 as:

$$|\psi_{\rm in}\rangle = \cos\left(\frac{\theta}{2}\right)|0\rangle_1 + e^{i\phi}\sin\left(\frac{\theta}{2}\right)|1\rangle_1. \tag{1}$$

Here the parameters $\theta \in [0,\pi]$ and $\phi \in [0,2\pi]$. Initially, a third party Charli prepared and distributed maximally entangled qubits 2 and 3, with the state $|\Phi_{23}^{+}\rangle = (|00\rangle_{23}+|11\rangle_{23})/\sqrt{2}$, to Alice and Bob. However, due to inevitable environmental effects, the entanglement degraded. When considering typical noise channels—such as phase damping, amplitude damping, and bit-flip channels—the density matrix of the two maximally entangled qubits degrades into the following X-type density matrix:

$$\rho_{23} = \begin{pmatrix} \varepsilon_{11} & 0 & 0 & \varepsilon_{14} \\ 0 & \varepsilon_{22} & \varepsilon_{23} & 0 \\ 0 & \varepsilon_{32} & \varepsilon_{33} & 0 \\ \varepsilon_{41} & 0 & 0 & \varepsilon_{44} \end{pmatrix}, \tag{2}$$

where the parameters $\varepsilon_{ij}$ depending on the channel parameters, will be calculated in detail in the following sections.

In the standard protocol of quantum teleportation, Alice first implements a CNOT gate on qubits 1 and 2, using qubit 1 as the control bit, thereby entangling qubit 1 and qubit 2. Subsequently, Alice implements a Hadamard gate on qubit 1, and performs projective measurements with the basises $\{|00\rangle, |01\rangle, |10\rangle, |11\rangle\}$ on qubits 1 and 2. She then transmits the measurement outcomes to Bob via classical communication. Based on the results, Bob performs corresponding unitary operations on qubit 3, reconstructing the output state density matrix as follows:

$$\rho_{\rm out} = \begin{pmatrix} \eta_1\cos^2\frac{\theta}{2} + \eta_2\sin^2\frac{\theta}{2} & \frac{1}{2}\sin\theta(\eta_3 e^{-i\phi} + \eta_4 e^{i\phi}) \\ \frac{1}{2}\sin\theta(\eta_3 e^{i\phi} + \eta_4 e^{-i\phi}) & \eta_2\cos^2\frac{\theta}{2} + \eta_1\sin^2\frac{\theta}{2} \end{pmatrix}, \tag{3}$$

with $\eta_1 = \varepsilon_{11} + \varepsilon_{44}$, $\eta_2 = \varepsilon_{22} + \varepsilon_{33}$, $\eta_3 = \varepsilon_{14} + \varepsilon_{41}$, and $\eta_4 = \varepsilon_{23} + \varepsilon_{32}$. In general, the concept of fidelity can be employed to evaluate the closeness of the output state reconstructed by Bob to the input state held by Alice. The fidelity is defined as $F = \left(\mathrm{Tr}\sqrt{\sqrt{\rho_{\rm in}}\rho_{\rm out}\sqrt{\rho_{\rm in}}}\right)^2$. Ideally, the fidelity can attain a value of 1, however, due to the influence of the noise channel, the fidelity will be significantly reduced.

In this work, we extend conventional protocols by incorporating non-Hermitian operations (the red-dashed-circular region in Fig. 1) on qubit 1 and investigate their beneficial effects on teleportation fidelity in the presence

of noisy channels. Specifically, we consider a simple form of non-Hermitian Hamiltonian, i.e.,

$$H_{\rm NH} = s\left(\sigma_x + ia\sigma_z\right), \tag{4}$$

where the real number $s$ is a scaling constant, and we set it to $s = 1$ throughout this paper. $a$ is a real parameter and $\sigma_i\,(i = x, y, z)$ are the Pauli operators. Notably, $H_{\rm NH}$ exhibits parity-time $\mathcal{PT}$ symmetry, satisfying $[H_{\rm NH}, \mathcal{PT}] = 0$ where $\mathcal{P}$, $\mathcal{T}$ denote the parity and time-reversal operators, respectively. For two-dimensional systems, the parity operator is $\sigma_x$ and the time-reversal operator acts as complex conjugation. The eigenvalues of $H_{\rm NH}$ are given by $\pm\omega$ where $\omega = \sqrt{1-a^2}$. Evidently, when $|a| \leq 1$, the non-Hermitian Hamiltonian $H_{\rm NH}$ possesses real eigenvalues; otherwise, the eigenvalues become purely imaginary. In the following analysis, we restrict our consideration to cases where $a \geq 0$. Consequently, the evolution operator $U_{\rm NH} = e^{-iH_{\rm NH}t}$ can be expressed as

$$U_{\rm NH} = \begin{pmatrix} \cos(\omega t) + \frac{a}{\omega}\sin(\omega t) & -\frac{i}{\omega}\sin(\omega t) \\ -\frac{i}{\omega}\sin(\omega t) & \cos(\omega t) - \frac{a}{\omega}\sin(\omega t) \end{pmatrix}. \tag{5}$$

Thus, Bob reconstructs the output state as

$$\rho_{\rm out}^{\rm NH} = \frac{1}{\mathcal{N}} \times \begin{pmatrix} \eta_1\mu_1\cos^2\frac{\theta}{2} + \eta_2\mu_2\sin^2\frac{\theta}{2} & \frac{1}{2}\sin\theta(\eta_3 e^{-i\phi} + \eta_4 e^{i\phi}) \\ \frac{1}{2}\sin\theta(\eta_3 e^{i\phi} + \eta_4 e^{-i\phi}) & \eta_2\mu_1\cos^2\frac{\theta}{2} + \eta_1\mu_2\sin^2\frac{\theta}{2} \end{pmatrix}, \tag{6}$$

with $\mathcal{N} = \mu_1\cos^2(\theta/2) + \mu_2\sin^2(\theta/2)$ and the parameters of $\mu_1$ and $\mu_2$ are determined by the eigenvalues of the non-Hermitian Hamiltonian $H_{\rm NH}$ as follows:

For $0 < a < 1$, the non-Hermitian Hamiltonian $H_{\rm NH}$ exhibits real eigenvalues, maintaining $\mathcal{PT}$-symmetry. In this regime, the associated parameters $\mu_1$ and $\mu_2$ are given by

$$\mu_{1,2} = \frac{1 - a^2\cos(2\omega t) \pm a\omega\sin(2\omega t)}{\omega^2}, \tag{7}$$

where $\mu_1$ corresponds to the "+" sign and $\mu_2$ corresponds to the "−"sign.

When $a > 1$, the eigenvalues of $H_{\rm NH}$ become complex, indicating the breaking of the $\mathcal{PT}$-symmetry. In this case the parameters $\mu_1$ and $\mu_2$ take the form

$$\mu_{1,2} = \frac{1 - a^2\cosh(2|\omega|t) \mp a|\omega|\sinh(2|\omega|t)}{\omega^2}, \tag{8}$$

with $\mu_1$ corresponding to the "−" sign and $\mu_2$ corresponding to the "+" sign.

The exceptional point $a = 1$ marks the threshold for $\mathcal{PT}$-symmetry breaking, where the eigenvalues transition from real to complex, accompanied by the degeneracy of the eigenstates. For $a = 0$, the non-Hermitian Hamiltonian $H_{\rm NH}$ reduces to the Hermitian Hamiltonian, restoring the standard quantum mechanical behavior. The expression in Eq. (6) provides a general result of the output state in the teleportation protocol, incorporating a non-Hermitian operation when the distributed entangled qubit pair is affected by noisy channels.

## III. TELEPORTATION FIDELITY

In this section, we will calculate the teleportation fidelity in detail [41], considering both the absence and presence of non-Hermitian operations. We will analyze three typical noise channels [42]: the phase damping, amplitude damping, and bit flip channels, respectively. In the absence of a non-Hermitian Hamiltonian, the fidelity between the output state $\rho_{\rm out}$ and the input state $\rho_{\rm in} = |\psi_{\rm in}\rangle\langle\psi_{\rm in}|$ [in Eq. (1)] is given by

$$F = \eta_1 + \frac{\eta_2 + \eta_3 - \eta_1}{2}\sin^2\theta, \tag{9}$$

with the coefficients $\eta_i$ determined by $\varepsilon_{ij}$ [under Eq. (3)]. This expression provides a general result for the teleportation fidelity corresponding to the X-type density matrix in Eq. (2).

When the non-Hermitian operation $U_{\rm NH}$ is introduced, the output state becomes $\rho_{\rm out}^{\rm NH}$ as given in Eq. (6). Consequently, the fidelity in this non-Hermitian protocol, denoted by $F^{\rm NH}$, can be derived for both the $\mathcal{PT}$-symmetric [using $\mu_{1,2}$ in Eq. (7)] and $\mathcal{PT}$-symmetry-breaking [using $\mu_{1,2}$ in Eq. (8)] cases. In order to clarify the impact of non-Hermitian operation on quantum teleportation, we define the difference between the two fidelities as

$$\Delta F \equiv F^{\rm NH} - F. \tag{10}$$

Clearly, when $\Delta F > 0$, the non-Hermitian operation plays a positive role to enhance the teleportation fidelity. In the following, we will calculate the special conditions under which non-Hermitian evolutions improve the teleportation fidelity for each of the three noise channels.

### A. Phase damping channel

We first consider the scenario where the entangled state $\left|\Phi_{23}^{+}\right\rangle$, shared by Alice and Bob, undergoes the phase damping channel and transforms into

$$\rho_{23}^{\rm PD} = \sum_{i,j=0}^{1} E_{ij}^{\rm PD}\left|\Phi_{23}^{+}\right\rangle\left\langle\Phi_{23}^{+}\right|(E_{ij}^{\rm PD})^{\dagger}, \tag{11}$$

where the maximally entangled state is defined as $|\Phi_{23}^{+}\rangle = (|00\rangle_{23} + |11\rangle_{23})/\sqrt{2}$. The Kraus operators describing the phase damping channel, locally performed on the two qubits, are given by $E_{ij}^{\rm PD} \equiv E_i^{\rm PD} \otimes E_j^{\rm PD}$ with $i(j) = 0, 1$, where

$$E_0^{\rm PD} = \begin{pmatrix} 1 & 0 \\ 0 & \sqrt{1-p_{\rm PD}} \end{pmatrix}, \quad E_1^{\rm PD} = \begin{pmatrix} 0 & 0 \\ 0 & \sqrt{p_{\rm PD}} \end{pmatrix}. \tag{12}$$

Here, $p_{\rm PD} \in [0, 1]$ is the damping parameter that characterizes the channel strength. Specially, $p_{\rm PD} = 0$ indicates the absence of noisy, while $p_{\rm PD} = 1$ represents to the strongest noisy effect. The coefficients of the density matrix in Eq. (2) become $\varepsilon_{11} = \varepsilon_{44} = 1/2$, and

$\varepsilon_{41} = \varepsilon_{14} = (1 - p_{\text{PD}})/2$. Therefore, the fidelity $F$ in Eq. (9) is obtained as

$$F_{\text{PD}} = 1 - \frac{1}{2} p_{\text{PD}} \sin^2\theta, \tag{13}$$

which clearly demonstrates that increasing channel strength reduces the teleporatation fidelity. The case of $p_{\text{PD}} = 1$ corresponds to the purely classical scenario, where no support is received from quantum entanglement.

By introducing the non-Hermitian operation, the fidelity between the output state $\rho_{\text{out}}^{\text{NH}}$ and the input state $\rho_{\text{in}}$ is expressed as

$$F_{\text{PD}}^{\text{NH}} = 1 + \frac{2 - 2p_{\text{PD}} - \mu_1 - \mu_2}{\mu_1 + \mu_2 + (\mu_1 - \mu_2)\cos\theta} \frac{\sin^2\theta}{2}, \tag{14}$$

which depends on the coefficients of the non-Hermitian Hamiltonian $\mu_{1,2}$ as defined in Eq. (7) or (8). Correspondingly, the difference between the non-Hermitian and Hermitian cases is expressed as

$$\Delta F_{\text{PD}} = F_{\text{PD}}^{\text{NH}} - F_{\text{PD}}. \tag{15}$$

In the following, we analytically and numerically analyze the difference of the fidelity in order to identify the conditions under which $\Delta F_{\text{PD}} > 0$, i.e., where non-Hermitian evolution provides an advantage in enhancing the teleportation fidelity.

By substituting the expressions of $F_{\text{PD}}$ and $F_{\text{PD}}^{\text{NH}}$ into Eq. (15) with the coefficients $\mu_{1,2}$ in Eq. (7), one can find the fidelity difference $\Delta F_{\text{PD}}$ exhibits periodic oscillations with time in the $\mathcal{PT}$-symmetric regime, and the period is

$$T_{\text{PD}} = \frac{\pi}{\omega}, \tag{16}$$

which is solely determined by the non-Hermitian parameter $\omega = \sqrt{1 - a^2}$. In each period, we derive that the time region for $\Delta F_{\text{PD}} > 0$ (for the case of $\cos\theta > 0$) should be

$$t_{\text{PD}} \in \frac{1}{\omega}\left(k\pi, \arctan\left[\frac{\omega p_{\text{PD}}\cos\theta}{a\,(1 - p_{\text{PD}})}\right] + k\pi\right), \tag{17}$$

with $k = 0, 1, 2, \cdots$. If $\cos\theta < 0$, the upper and lower bounds of the region should be swapped. The existence of this time region indicates that, as long as the noisy channel effect considered for $0 < p_{\text{PD}} < 1$ and $\cos\theta \neq 0$, the protocol with $\mathcal{PT}$-symmetric non-Hermitian operations can provide better teleportation fidelity than the conventional protocol (without non-Hermitian operations). Moreover, for larger channel strength $p_{\text{PD}}$, the advantageous interval of $t_{\text{PD}}$ widens, implying that the positive effects of non-Hermitian operations become more pronounced in these cases. The expression also reveals that for approximately $(p_{\text{PD}}\cos\theta)/(1 - p_{\text{PD}}) > 3$, increasing the non-Hermitian parameter $a$ may monotonically increase the width of $t_{\text{PD}}$.

We numerically calculate the fidelity difference and present the results in Fig. 2. The parameters of the state to be teleported are chosen as $\theta = \pi/3$ and $\phi = 0$. We then introduce non-Hermitian operators and calculate $\Delta F_{\text{PD}}$ as a function of time $t$. First, the cases of the non-Hermitian Hamitonian parameter $a = 0.2$ and $a = 0.5$ are shown in Fig. 2 (a) and (b) respectively, where the non-Hermitian Hamiltonian holds $\mathcal{PT}$ symmetry. In addition, we examine different phase-damping channel strengths $p_{\text{PD}}$. The results reveal oscillations of $\Delta F_{\text{PD}}$ over time, and the regions where $\Delta F_{\text{PD}} > 0$ confirm the analytical predictions in Eq. (17). As the channel strength $p_{\text{PD}}$ increases, the amplitude of $\Delta F_{\text{PD}}$ increases, and the regions where $\Delta F_{\text{PD}} > 0$ expand. However, for the case $p_{\text{PD}} = 0$, $\Delta F_{\text{PD}}$ remains negative. This implies that the non-Hermitian teleportation protocol demonstrates its advantage more clearly when the noisy channel strength is significant. By comparing Fig. 2 (a) and Fig. 2 (b), we observe that increasing non-Hermitian parameter $a$ extends the oscillation period $T_{\text{PD}}$ and enhances the amplitude of $\Delta F_{\text{PD}}$.

When the non-Hermitian parameter increases into the $\mathcal{PT}$-symmetry-breaking regime, i.e., $a > 1$, the fidelity difference $\Delta F_{\text{PD}}$ no longer exhibits periodic oscillations but instead converges to a steady value, given by

$$\lim_{t\to\infty}(\Delta F_{\text{PD}}) = \frac{1}{2}\left(p_{\text{PD}} - \frac{a}{a + \sqrt{a^2 - 1}\cos\theta}\right)\sin^2\theta. \tag{18}$$

This implies that under the condition

$$\left(1 + \cos\theta\frac{\sqrt{a^2 - 1}}{a}\right) p_{\text{PD}} > 1, \tag{19}$$

the steady value satisfies $\lim_{t\to\infty}(\Delta F_{\text{PD}}) > 0$. For a certain input state and noise channel, the relationship above allows the selection of an appropriate non-Hermitian parameter to enhance the teleportation fidelity, i.e., $\Delta F_{\text{PD}} > 0$. Fig. 2 (c) illustrates the time evolution of $\Delta F_{\text{PD}}$ driven by the non-Hermitian Hamiltonian with $a = 4$, considering different channel parameters $p_{\text{PD}} = 0,\ 0.7,\ 0.9$. For a strong channel $p_{\text{PD}} = 0.9$ (red dash-dotted line), $\Delta F_{\text{PD}}$ rapidly increases to a steady value of approximately 0.085 which is consistent with the analytical results in Eq. (18).

### B. Amplitude damping noise channel

We proceed to investigate the case of amplitude damping channel. The entangled state $\rho_{23}$ shared by Alice and Bob evolves into

$$\rho_{23}^{\text{AD}} = \sum_{i,j=0}^{1} E_{ij}^{\text{AD}} \left|\Phi_{23}^{+}\right\rangle \left\langle\Phi_{23}^{+}\right| (E_{ij}^{\text{AD}})^{\dagger}, \tag{20}$$

where the Kraus operators $E_{ij}^{\text{AD}} = E_i^{\text{AD}} \otimes E_j^{\text{AD}}$, with $i(j) = 0, 1$, are defined as

$$E_0^{\text{AD}} = \begin{pmatrix} 1 & 0 \\ 0 & \sqrt{1 - p_{\text{AD}}} \end{pmatrix}, \quad E_1^{\text{AD}} = \begin{pmatrix} 0 & \sqrt{p_{\text{AD}}} \\ 0 & 0 \end{pmatrix}, \tag{21}$$

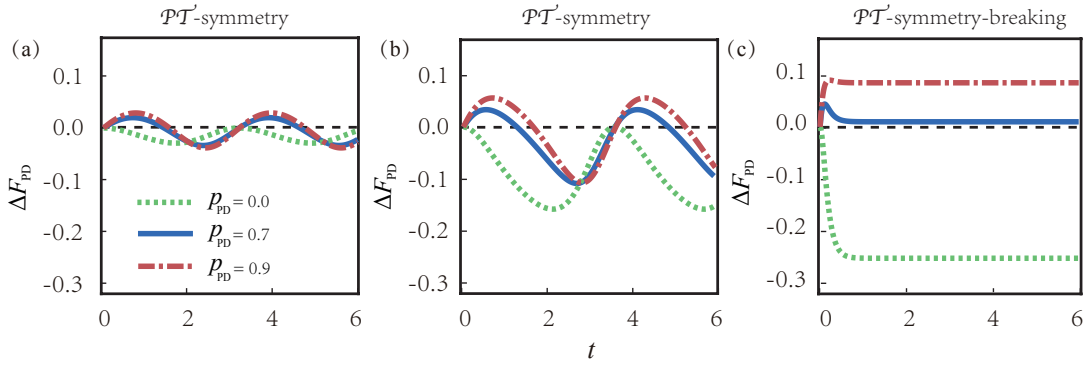


Figure 2. Time evolution of the fidelity difference $\Delta F_{\rm PD}$ under the influence of non-Hermitian operators for varying phase damping parameters $p_{\rm PD}$ and non-Hermitian parameters $a$. The phase damping noise channel strength is set to $p_{\rm PD}=0$ (green dashed line), $p_{\rm PD}=0.7$ (blue solid line), and $p_{\rm PD}=0.9$ (red dash-dotted line), while the non-Hermitian parameter takes values $a=0.2$ (a), $a=0.5$ (b), and $a=4$ (c). The results highlight the impact of $\mathcal{PT}$-symmetric and symmetry-breaking operations on the teleportation fidelity.

with the amplitude damping parameter $p_{\rm AD}\in[0,1]$. Then the coefficients in Eq. (2) become $\varepsilon_{11}=\left(1+p_{\rm AD}^2\right)/2$, $\varepsilon_{22}=\varepsilon_{33}=\left(1-p_{\rm AD}\right)p_{\rm AD}/2$, $\varepsilon_{44}=\left(1-p_{\rm AD}\right)^2/2$, and $\varepsilon_{41}=\varepsilon_{14}=\left(1-p_{\rm AD}\right)/2$. Therefore, one can obtain the fidelity in Eq. (9) as

$$F_{\rm AD}=1-p_{\rm AD}+p_{\rm AD}^2+(\frac{1}{2}-p_{\rm AD})p_{\rm AD}\sin^2\theta. \tag{22}$$

Obviously, the dependence of $F_{\rm AD}$ on the parameter $p_{\rm AD}$ is not monotonic. In order to demonstrate the advantages of the quantum protocol, in the following calculations, we choose the values of the parameter $\theta$ and $p_{\rm AD}$ such that the fidelity $F_{\rm AD}$ of the standard quantum teleportation protocol exceeds that of the classical scheme, i.e., $p_{\rm AD}=1$. Therefore, we select the parameters based on the following condition:

$$\sin^2\theta>\frac{2p_{\rm AD}}{1+2p_{\rm AD}}. \tag{23}$$

Whereas, in the non-Hermitian protocol, the fidelity between the output state $\rho_{\rm out}^{\rm NH}$ and the input state $\rho_{\rm in}$ is given by

$$\begin{aligned}F_{\rm AD}^{\rm NH}&=1-p_{\rm AD}+p_{\rm AD}^2\\&+\frac{2-2p_{\rm AD}+(2p_{\rm AD}-2p_{\rm AD}^2-1)(\mu_1+\mu_2)}{\mu_1+\mu_2+(\mu_1-\mu_2)\cos\theta}\frac{\sin^2\theta}{2},\end{aligned} \tag{24}$$

with the coefficients $\mu_{1,2}$ defined in Eq. (7) or (8).

The fidelity difference is

$$\Delta F_{\rm AD}=F_{\rm AD}^{\rm NH}-F_{\rm AD}. \tag{25}$$

In this case we can calculate the fidelity difference $\Delta F_{\rm AD}$ in detail and clarify the conditions required to achieve $\Delta F_{\rm PD}>0$.

When the parameter $a<1$ of the non-Hermitian Hamiltonian places the system in the $\mathcal{PT}$-symmetric regime, the fidelity difference $\Delta F_{\rm AD}$ displays periodic oscillations over time with a period $T_{\rm AD}=\pi/\omega$. Within each period, $\Delta F_{\rm AD}$ remains positive for times $t$ satisfying the constraint:

$$t_{\rm AD}\in\frac{1}{\omega}\left(k\pi,\arctan\left[\frac{p_{\rm AD}(2p_{\rm AD}-1)\omega\cos\theta}{a(1-p_{\rm AD})}\right]+k\pi\right). \tag{26}$$

The numerical results are shown in Fig. 3. The values of the parameters $\theta$, $\phi$, $a$, $p_{\rm AD}$ are chosen the same as those in Fig. 2. Similar phenomena are found in both figures, except that in the $\mathcal{PT}$-symmetry regime, such as $a=0.2$ [Fig. 3 (a)] and 0.5 [Fig. 3 (b)], the time intervals for $\Delta F_{\rm AD}>0$ are shorter in comparison to those in Fig. 2. This difference can be understood by comparing the analytical results in Eqs. (17) and (26). For channel values $0<p_{\rm AD(PD)}<1$, it is consistently observed that the interval of $t_{\rm PD}$ is broader than that for $t_{\rm AD}$.

When the non-Hermitian parameter $a>1$, the $\mathcal{PT}$ symmetry is broken, then the fidelity difference $\Delta F_{\rm AD}$ rapidly converges to its steady value:

$$\begin{aligned}\lim_{t\to\infty}(\Delta F_{\rm AD})&=\frac{1}{2}p_{\rm AD}(2p_{\rm AD}-1)\sin^2\theta\\&+\frac{a(2p_{\rm AD}-2p_{\rm AD}^2-1)}{2(a+\sqrt{a^2-1}\cos\theta)}\sin^2\theta.\end{aligned} \tag{27}$$

Here, it is evident that different values of the channel parameter $p_{\rm AD}$ correspond to distinct steady values of $\Delta F_{\rm AD}$. The dependence of the steady $\Delta F_{\rm AD}$ on the parameters $p_{\rm AD}$, $\theta$, and $a$ differs significantly from that of $\Delta F_{\rm PD}$ in Eq. (18). Additionally, we derive the conditions ensuring the steady value $\lim_{t\to\infty}(\Delta F_{\rm AD})>0$. For $p_{\rm AD}=1/2$, there should be

$$a+\cos\theta\sqrt{a^2-1}<0, \tag{28}$$

while for $p_{\rm AD}\neq1/2$, the condition becomes

$$p_{\rm AD}(2p_{\rm AD}-1)\sqrt{a^2-1}\cos\theta>a(1-p_{\rm AD}). \tag{29}$$

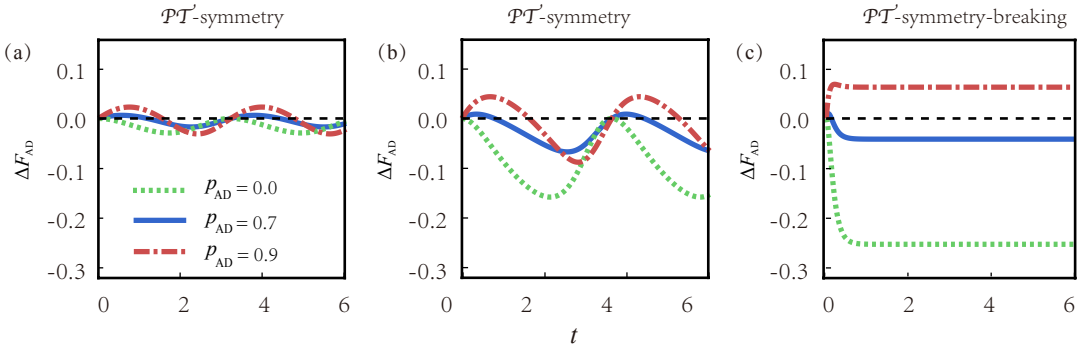


Figure 3. Time evolution of the fidelity difference $\Delta F_{\rm AD}$ under the influence of non-Hermitian operations for varying for varying amplitude damping noise channel strength $p_{\rm PD}$ and non-Hermitian parameters $a$. The amplitude damping noise channel strength is set to $p_{\rm PD}=0$ (green dashed line), $p_{\rm PD}=0.7$ (blue solid line), and $p_{\rm PD}=0.9$ (red dash-dotted line), while the non-Hermitian parameter takes values $a=0.2$ (a), $a=0.5$ (b), and $a=4$ (c).

The numerical results depicted in Fig. 3 (c) illustrate the time evolution of $\Delta F_{\rm AD}$ for $a=4$ with different $p_{\rm AD}=0, 0.7, 0.9$. In contrast to Fig. 2 (c), a notable difference is observed: for $p_{\rm AD}=0.7$, there is virtually no time interval where $\Delta F_{\rm AD}>0$. This implies that the non-Hermitian approach is significantly less effective for the amplitude damping channel compared to the phase damping channel.

### C. Bit flip noise channel

In this section, we consider the case of bit flip noise channel, then the entangled state $\rho_{23}$, shared by Alice and Bob, evolves into a mixed state, i.e.,

$$\rho_{23}^{\rm BF}=\sum_{i,j=0}^{1}E_{ij}^{\rm BF}\left|\Phi_{23}^{+}\right\rangle\left\langle\Phi_{23}^{+}\right|(E_{ij}^{\rm BF})^{\dagger}, \tag{30}$$

where the Kraus operators $E_{ij}^{\rm BF}=E_{i}^{\rm BF}\otimes E_{j}^{\rm BF}$ with $i(j)=0,1$ are defined in tensor product form as

$$E_{0}^{\rm BF}=\sqrt{p_{\rm BF}}\begin{pmatrix}1&0\\0&1\end{pmatrix},\ E_{1}^{\rm BF}=\sqrt{1-p_{\rm BF}}\begin{pmatrix}0&1\\1&0\end{pmatrix}, \tag{31}$$

with the bit flip probability $p_{\rm BF}\in[0,1]$, where $p_{\rm BF}=1/2$ corresponds to the maximal channel strength. The coefficients in Eq. (2) then become $\varepsilon_{11}=\varepsilon_{14}=\varepsilon_{41}=\varepsilon_{44}=\frac{1}{2}-p_{\rm BF}+p_{\rm BF}^2$ and $\varepsilon_{22}=\varepsilon_{23}=\varepsilon_{32}=\varepsilon_{33}=p_{\rm BF}-p_{\rm BF}^2$. The fidelity in Eq. (9) is derived as

$$F_{\rm BF}=1-2p_{\rm BF}+2p_{\rm BF}^2+(p_{\rm BF}-p_{\rm BF}^2)\sin^2\theta. \tag{32}$$

We find that for all the values of $\theta\in[0,\pi]$, as long as $p_{\rm BF}\neq 1/2$, the teleportation fidelity $F_{\rm BF}$ consistently has $F_{\rm BF}>F_{\rm BF}|_{p_{\rm BF}=1/2}$. This indicates that the quantum protocol (when $p_{\rm BF}\neq 1/2$) achieve a higher fidelity than the classical protocol when the noisy channel reaches its maximal strength $p_{\rm BF}=1/2$, which completely destroys quantum entanglement.

Subsequently, the fidelity in the non-Hermitian protocol is computed between the output state $\rho_{\rm out}^{\rm NH}$ and the input state $\rho_{\rm in}$ as

$$\begin{aligned}F_{\rm BF}^{\rm NH}&=1-2p_{\rm BF}-2p_{\rm BF}^2\\&+\frac{1-2p_{\rm BF}(1-p_{\rm BF})\left(\cos 2\phi-1\right)}{\mu_1+\mu_2+(\mu_1-\mu_2)\cos\theta}\sin^2\theta\\&-\frac{(2p_{\rm BF}-1)^2(\mu_1+\mu_2)}{\mu_1+\mu_2+(\mu_1-\mu_2)\cos\theta}\frac{\sin^2\theta}{2},\end{aligned} \tag{33}$$

with the coefficients $\mu_{1,2}$ defined in Eq. (7) or (8). A distinctive feature of $F_{\rm BF}^{\rm NH}$ compared to $F_{\rm PD}^{\rm NH}$ [in Eq. (14)] and $F_{\rm AD}^{\rm NH}$ [in Eq. (24)] is its explicit dependence on parameter $\phi$, in addition to the parameters $p_{\rm BF}$, $\mu_{1,2}$, and $\theta$. When averaging the fidelity over all possible $\phi$, $F_{\rm BF}^{\rm NH}$ simplifies to

$$\begin{aligned}F_{\rm BF}^{\rm NH}&=1-2p_{\rm BF}+2p_{\rm BF}^2\\&+\frac{1+(2p_{\rm BF}-1)^2\left(1-\mu_1-\mu_2\right)}{\mu_1+\mu_2+(\mu_1-\mu_2)\cos\theta}\frac{\sin^2\theta}{2}.\end{aligned} \tag{34}$$

Here we focus on the fidelity difference $\Delta F_{\rm BF}$ defined as

$$\Delta F_{\rm BF}=F_{\rm BF}^{\rm NH}-F_{\rm BF}, \tag{35}$$

which is a function of $\theta$ by using Eqs. (32) and (34). In the $\mathcal{PT}$-symmetry regime, where the non-Hermitian Hamiltonian parameter $a<1$, $\Delta F_{\rm BF}$ displays as a periodic function of time, similar to $\Delta F_{\rm PD}$ and $\Delta F_{\rm AD}$ with the same period $T_{\rm BF}=\pi/\omega$. Within each period, the time interval corresponding to positive values of $\Delta F_{\rm BF}>0$ (for the case of $\cos\theta>0$) is given by

$$t_{\rm BF}\in\frac{1}{\omega}\left(\arctan\left[\frac{2\omega p_{\rm BF}(p_{\rm BF}-1)\cos\theta}{a(1-2p_{\rm BF}+2p_{\rm BF}^2)}\right]+k\pi,k\pi\right), \tag{36}$$

while for the case of $\cos\theta<0$, the upper and lower bound should be swapped. It can be observed that the width of $t_{\rm BF}$ is larger than that of $t_{\rm PD}$ in the phase damping channel [Eq. (17)] for $0<p_{\rm BF(PD)}<1/2$, but it becomes

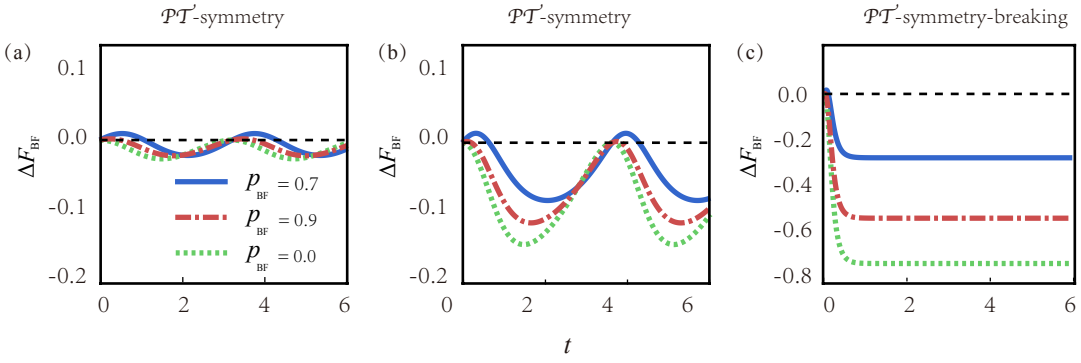


Figure 4. Time evolution of the fidelity difference $\Delta F_{\rm BF}$ under the influence of non-Hermitian operators for varying bit flip noise channel strength $p_{\rm BF}$ and non-Hermitian parameters $a$. The bit flip noise channel strength is set to $p_{\rm BF} = 0$ (green dashed line), $p_{\rm BF} = 0.7$ (blue solid line), and $p_{\rm BF} = 0.9$ (red dash-dotted line), while the non-Hermitian parameter takes values $a = 0.2$ (a), $a = 0.5$ (b), and $a = 4$ (c).

equal or smaller when $1/2 \leq p_{\rm BF(PD)} < 1$. This is verified by comparing the results in Fig. 2 and Fig. 4. Additionally, the width of $t_{\rm BF}$ in Eq. (36) is larger than that of $t_{\rm AD}$ in the amplitude damping channel [Eq. (26)] for $0 < p_{\rm BF(AD)} \lesssim 0.6806$. However, beyond this region, i.e., for $0.6806 \lesssim p_{\rm BF(AD)} < 1$, the width of $t_{\rm BF}$ becomes smaller than that of $t_{\rm AD}$.

When the non-Hermitian parameter exceeds $a > 1$, the $\mathcal{PT}$ symmetry is broken. In this regime, the fidelity difference $\Delta F_{\rm BF}$ no longer exhibits periodic oscillations but instead converges to a steady value:

$$\lim_{t\to\infty}(\Delta F_{\rm BF}) = \sin^2\theta \times \left[p_{\rm BF}(p_{\rm BF}-1) - \frac{a(2p_{\rm BF}-1)^2}{2(a+\sqrt{a^2-1}\cos\theta)}\right]. \tag{37}$$

It can be shown that the steady value in this case is always negative, i.e., $\lim_{t\to\infty}(\Delta F_{\rm BF}) < 0$.

The numerical results are presented in Fig. 4. The input state parameters are chosen as $\theta = 2\pi/3$ and $\phi = 0$. We numerically investigate the effect of non-Hermitian operators on the teleportation fidelity under the initial influence of a bit flip noise channel, as shown in Fig. 4. When the non-Hermitian parameter $a < 1$, the non-Hermitian Hamiltonian displays $\mathcal{PT}$-symmetric characteristics. The time evolution of the fidelity difference $\Delta F_{\rm BF}$ is plotted for various bit flip noise channel strengths $p_{\rm BF}$, with $a = 0.2$ in Fig. 4 (a) and $a = 0.5$ in Fig. 4 (b). Under $\mathcal{PT}$-symmetric operations, $\Delta F_{\rm BF}$ exhibits periodic oscillations, with the oscillation period determined by $T_{\rm BF} = \pi/\omega$. The existence of the time interval indicates that $\mathcal{PT}$-symmetric operations improve the fidelity of quantum teleportation. Different channel parameters $p_{\rm BF}$ influence the width of the time interval $t_{\rm BF}$ defined in Eq. (36) and the amplitude of $\Delta F_{\rm BF}$. Fig. 4 (c) depicts the time evolution of $\Delta F_{\rm BF}$ for $a = 4$. In this case, the steady value of $\Delta F_{\rm BF}$ never exceeds zero, which aligns with the analysis results.

## IV. QUANTUM FISHER INFORMATION

Quantum Fisher information (QFI) serves as the fundamental quantity that defines the precision limit for parameter estimation [43–51]. As such, QFI represents a critical resource that merits careful consideration in the context of quantum teleportation. In this work, the teleported QFI will be thoroughly examined as an essential and complementary aspect of our investigation.

Given the spectral decomposition of a density matrix, $\rho = \sum_n \lambda_n |\psi_n\rangle\langle\psi_n|$, the QFI for the parameter $\alpha$ can be calculated as

$$\mathcal{F}_\alpha = \sum_{\substack{n \\ \lambda_n\neq 0}} \frac{(\partial_\alpha \lambda_n)^2}{\lambda_n} + \sum_{\substack{n,m \\ \lambda_n+\lambda_m\neq 0}} \frac{2(\lambda_n-\lambda_m)^2}{\lambda_n+\lambda_m} |\langle\psi_n|\partial_\alpha\psi_m\rangle|^2 . \tag{38}$$

Here, the first term can be viewed as the counterpart of the classical Fisher information, as it only contains the derivatives of the eigenvalues, which can be regarded as the counterpart of the probability distribution, and the second term is purely quantum. On the other hand, a parameterized state $\rho_\alpha$ in two-dimensional systems can be represented in terms of the Bloch vector as $\rho_\alpha = \frac{1}{2}(\hat{\mathbb{I}} + \vec{r}_\alpha \cdot \hat{\vec{\sigma}})$, where $\vec{r}_\alpha = (r_{1\alpha}, r_{2\alpha}, r_{3\alpha})^{\rm T}$ with $r_{i\alpha} = {\rm Tr}(\rho_\alpha \hat{\sigma}_i)$. Then by using the formula of QFI shown in [52], i.e.,

$$\mathcal{F} = \begin{cases} |\partial_\alpha \vec{r}_\alpha|^2 + \frac{(\vec{r}_\alpha\cdot\partial_\alpha\vec{r}_\alpha)^2}{1-|\vec{r}_\alpha|^2}, & |\vec{r}_\alpha| < 1, \\ |\partial_\alpha \vec{r}_\alpha|^2, & |\vec{r}_\alpha| = 1. \end{cases} \tag{39}$$

Next, we focus on the teleportation of the QFI encoded in the input state $|\psi_{\rm in}\rangle$ defined in Eq. (1). Within the teleportation framework, the initial entangled qubit pair shared by Alice and Bob is subjected to a noisy channel, with the phase-damping noise channel serving as the primary example in this analysis. We explore the influence of non-Hermitian operations encompassing both $\mathcal{PT}$-symmetric and $\mathcal{PT}$-symmetry-breaking Hamiltonians, on the teleported QFI associated with the parameters $\phi$ and $\theta$, respectively.

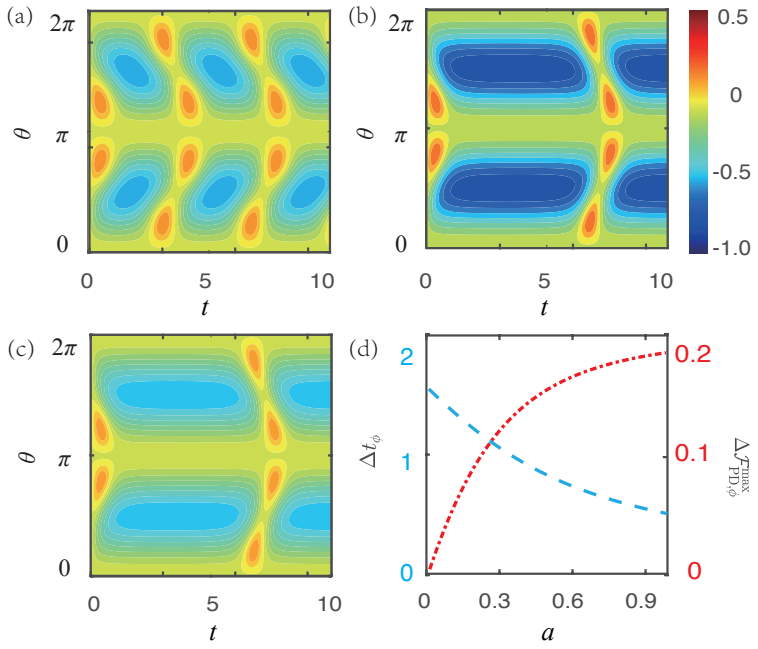


Figure 5. (a), (b), and (c) illustrate the variation of the quantum Fisher information difference $\Delta\mathcal{F}_{\mathrm{PD},\phi}$ as a function of time $t$ and the state parameter $\theta$ under $\mathcal{PT}$-symmetric operations. The non-Hermitian parameter $a$ and noise channel strength $p_{\mathrm{PD}}$ are set as follows: (a) $a = 0.5$, $p_{\mathrm{PD}} = 0.9$; (b) $a = 0.9$, $p_{\mathrm{PD}} = 0.9$; (c) $a = 0.9$, $p_{\mathrm{PD}} = 0.5$. For the specific case of $\theta = 2\pi/3$, (d) shows how the time interval width $\Delta t_\phi|_{\Delta\mathcal{F}_{\mathrm{PD},\phi}>0}$ (blue dashed line) and its corresponding maximum value $\Delta\mathcal{F}^{\max}_{\mathrm{PD},\phi}$ (red dotted line) depend on the non-Hermitian parameter $a$ with $p_{\mathrm{PD}} = 0.9$.

### A. Teleported QFI of Parameter $\phi$

In the conventional teleportation protocol without non-Hermitian operators, the teleported QFI for the parameter $\phi$ is given by

$$\mathcal{F}_{\mathrm{PD},\phi} = (1 - p_{\mathrm{PD}})^2 \sin^2\theta, \tag{40}$$

where the channel parameter $p_{\mathrm{PD}}$ corresponds to the phase damping channel in the Eq. (21). Comparing this result with the teleportation fidelity in Eq. (12), a notable distinction emerges between the teleportation fidelity and teleported QFI for $\phi$. For instance, in the case of the strongest noisy channel with $p_{\mathrm{PD}} = 1$, the teleportation fidelity becomes $F_{\mathrm{PD}} = 1 - \sin^2\theta/2$, whereas the teleported QFI for $\phi$ vanishes, i.e., $\mathcal{F}_{\mathrm{PD},\phi} = 0$. This indicates that while Bob can partially reconstruct the state under the maximal influence of the noisy channel, he may not be able to extract the necessary QFI.

Upon introducing non-Hermitian operators, the teleported QFI becomes

$$\mathcal{F}^{\mathrm{NH}}_{\mathrm{PD},\phi} = \frac{(1 - p_{\mathrm{PD}})^2 \sin^2\theta}{(\mu_1 \cos^2\frac{\theta}{2} + \mu_2 \sin^2\frac{\theta}{2})^2}, \tag{41}$$

where the coefficients $\mu_{1,2}$ are associated with the non-Hermitian Hamiltonian, as defined in Eq. (7) or (8). While the teleported QFI remains $\mathcal{F}^{\mathrm{NH}}_{\mathrm{PD},\phi} = 0$ when $p_{\mathrm{PD}} = 1$, the introduction of non-Hermitian operations enables the extraction of more QFI for other values of $p_{\mathrm{PD}}$. To quantify the impact of non-Hermitian operations on the teleported QFI, we define the QFI difference as

$$\Delta\mathcal{F}_{\mathrm{PD},\phi} \equiv \mathcal{F}^{\mathrm{NH}}_{\mathrm{PD},\phi} - \mathcal{F}_{\mathrm{PD},\phi}. \tag{42}$$

In the subsequent analysis, we compute $\Delta\mathcal{F}_{\mathrm{PD},\phi}$ for both $\mathcal{PT}$-symmetric and $\mathcal{PT}$-symmetry-breaking non-Hermitian operations, and identify the conditions under which $\Delta\mathcal{F}_{\mathrm{PD},\phi} > 0$, indicating that non-Hermitian operations enhance the teleported QFI.

#### 1. $\mathcal{PT}$-symmetric operations

When the non-Hermitian parameter $a < 1$, the non-Hermitian Hamiltonian maintains $\mathcal{PT}$ symmetry. In this regime, the QFI difference $\Delta\mathcal{F}_{\mathrm{PD},\phi}$ exhibits periodic oscillations [see Fig. (5)] with a period $T_\phi = \pi/\omega$. The oscillation period is determined solely by the non-Hermitian parameter $a$ and remains unaffected by the noise channel strength $p_{\mathrm{PD}}$. This is supported by the numerical simulation results shown in Figs. 5 (a) and (b), where for the same $p_{\mathrm{PD}} = 0.9$, a larger value of $a$ provides a longer oscillation period. On the other hand, comparing Figs. 5 (b) and (c), when the same value of $a$ (e.g., $a = 0.9$) is considered, varying $p_{\mathrm{PD}}$ does not alter the oscillation period, but only affects the amplitude of $\Delta\mathcal{F}_{\mathrm{PD},\phi}$.

Let us calculate in detail the time interval $t_\phi$ for which

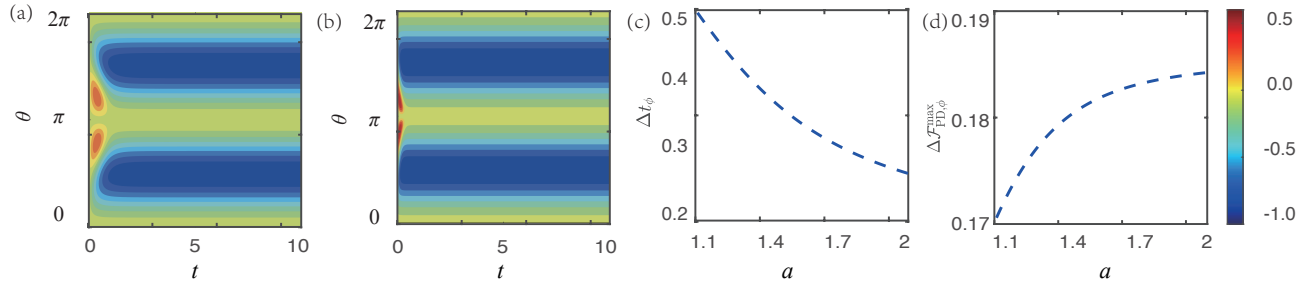


Figure 6. (a) and (b) illustrate the variation of the quantum Fisher information difference $\Delta\mathcal{F}_{\mathrm{PD},\phi}$ with respect to time $t$ and the state parameter $\theta$ under $\mathcal{PT}$-symmetry-breaking operations, with the non-Hermitian parameter set to $a = 1.1$ and $a = 4.0$, respectively. Taking the parameter $\theta = 2\pi/3$ as an example, (c) depicts the width of the time interval $\Delta t_\phi\big|_{\Delta\mathcal{F}_{\mathrm{PD},\phi}>0}$ as a function of the non-Hermitian parameter $a$, while (d) presents the maximum value $\Delta\mathcal{F}^{\max}_{\mathrm{PD},\phi}$ of $\Delta\mathcal{F}_{\mathrm{PD},\phi}$ as a function of $a$ with $p_{\mathrm{PD}} = 0.9$.

$\Delta\mathcal{F}_{\mathrm{PD},\phi} > 0$, given by

$$t_\phi \in \frac{1}{\omega}\left(k\pi,\, k\pi + \arctan[\frac{\omega}{a}\cos\theta]\right), \tag{43}$$

where $\omega = \sqrt{1-a^2}$, $\cos\theta > 0$, and $k = 0, 1, 2, \cdots$. For the case of $\cos\theta < 0$, the upper and lower bound should be swapped. The existence of this time region indicates that $\mathcal{PT}$-symmetric operations enhance the teleported QFI compared to the conventional protocol. Notably, the time interval $t_\phi$ is independent of the channel parameter $p_{\mathrm{PD}}$. This conclusion is further verified by comparing the numerical results shown in Figs. 5 (b) and (c). Moreover, based on the Eq. (43), we find that the width of the width of the time interval $\Delta t_\phi\big|_{\Delta\mathcal{F}_{\mathrm{PD},\phi}>0}$ gradually decreases as $a$ increases, which is verified by the numerical results of the blue dashed line in Fig. 5 (d).

Through a comprehensive comparative analysis of the time intervals $t_\phi$ for QFI in Eq. (43) and $t_{\mathrm{PD}}$ for teleportation fidelity in Eq. (17), we observe significant differences between them. Specifically, the width of $t_{\mathrm{PD}}$ is influenced by the channel parameter $p_{\mathrm{PD}}$, whereas the width of $t_\phi$ remains independent of it. Upon deeper examination, we find that for $p_{\mathrm{PD}} < 1/2$, the width of $t_\phi$ exceeds that of $t_{\mathrm{PD}}$; conversely, for $p_{\mathrm{PD}} > 1/2$, the width of $t_\phi$ becomes smaller. In the special case where $p_{\mathrm{PD}} = 1/2$, the widths of $t_\phi$ and $t_{\mathrm{PD}}$ are identical.

We can also derive the maximum value of $\Delta\mathcal{F}_{\mathrm{PD},\phi}$ as

$$\Delta\mathcal{F}^{\max}_{\mathrm{PD},\phi} = \frac{(1-p_{\mathrm{PD}})^2\sin^2\theta\omega^4}{\left(1-a\sqrt{a^2\sin^2\theta+\cos^2\theta}\right)^2} - (1-p_{\mathrm{PD}})^2\sin^2\theta, \tag{44}$$

which demonstrates that the value of $\Delta\mathcal{F}^{\max}_{\mathrm{PD},\phi}$ increases with larger values of $a$ but decreases with larger values of $p_{\mathrm{PD}}$. Moreover, it can be proved that the maximal value occurs at the midpoint of each time interval. As illustrated by the red dotted line in Fig. 5 (d), taking $p_{\mathrm{PD}} = 0.9$ as an example, the maximum value $\Delta\mathcal{F}^{\max}_{\mathrm{PD},\phi}$ exhibits a monotonically decreasing function with respect of the parameter $a$.

### 2. $\mathcal{PT}$-symmetry-breaking operations

When the non-Hermitian parameter $a > 1$, the non-Hermitian Hamiltonian exhibits $\mathcal{PT}$-symmetry breaking, then $\omega = \sqrt{1-a^2}$ becomes an imaginary number. In this case, the periodic oscillations of QFI disappear. However, there is a short time interval during which $\Delta\mathcal{F}_{\mathrm{PD},\phi}$ is larger than zero, and the time interval is given by

$$t_\phi \in \left(0, \frac{1}{2|\omega|}\ln\left[\frac{a-|\omega|\cos\theta}{a+|\omega|\cos\theta}\right]\right), \tag{45}$$

which requires $\cos\theta < 0$. The maximum value of $\Delta\mathcal{F}_{\mathrm{PD},\phi}$, denoted as $\Delta\mathcal{F}^{\max}_{\mathrm{PD},\phi}$, follows the same expression as Eq. (44). For a longer time evolution, the non-Hermitian QFI $\mathcal{F}_{\mathrm{PD},\phi}$ tends to zero, and thus the QFI difference $\Delta\mathcal{F}_{\mathrm{PD},\phi}$ converges to a steady value, i.e.,

$$\lim_{t\to\infty}(\Delta\mathcal{F}_{\mathrm{PD},\phi}) = -(1-p_{\mathrm{PD}})^2\sin^2\theta, \tag{46}$$

which is clearly negative. The analytical results are corroborated by numerical simulations presented in Fig. 6, where different non-Hermitian parameters are considered: $a = 1.1$ in Fig. 6 (a) and $a = 4.0$ in Fig. 6 (b). Taking $\theta = 2\pi/3$ as an example, Fig. 6 (c) illustrates the width of the time interval $t_\phi$ denoted by $\Delta t_\phi\big|_{\Delta\mathcal{F}_{\mathrm{PD},\phi}>0}$ gradually decreases as $a$ increases, while Fig. 6 (d) shows that the maximum value $\Delta\mathcal{F}^{\max}_{\mathrm{PD},\phi}$ (with $p_{\mathrm{PD}} = 0.9$) increases with $a$.

## B. Teleported QFI of Parameter $\theta$

In the absence of non-Hermitian operators, we find that the QFI ($\mathcal{F}_{\mathrm{PD},\theta}$) of the parameter $\theta$ is a constant number, i.e., $\mathcal{F}_{\mathrm{PD},\theta} = 1$, which is independent of the channel parameter. The phase-damping channel, acting on the entangled qubits initially distributed to Alice and Bob, does not influence the teleported QFI of $\theta$. This implies that the QFI can be fully transmitted through

the classical channel in this case. However, when non-Hermitian operators are introduced, the QFI of $\theta$ becomes

$$\mathcal{F}_{\mathrm{PD},\theta}^{\mathrm{NH}} = \frac{\mu_1\mu_2}{\left(\mu_1\cos^2\frac{\theta}{2}+\mu_2\sin^2\frac{\theta}{2}\right)^2}, \tag{47}$$

where $\mu_{1,2}$ are the coefficients of the non-Hermitian Hamiltonian defined in Eq. (7) or (8). Unlike the $\mathcal{F}_{\mathrm{PD},\theta}$, $\mathcal{F}_{\mathrm{PD},\theta}^{\mathrm{NH}}$ is no longer a constant. Notably, both of $\mathcal{F}_{\mathrm{PD},\theta}$ and $\mathcal{F}_{\mathrm{PD},\theta}^{\mathrm{NH}}$ remain independent on the channel parameter, which contrast with the behavior of the teleported QFI of $\phi$. To investigate the conditions under which non-Hermitian evolution enhances the QFI, we define the difference in QFI as:

$$\Delta\mathcal{F}_{\mathrm{PD},\theta} \equiv \mathcal{F}_{\mathrm{PD},\theta}^{\mathrm{NH}} - \mathcal{F}_{\mathrm{PD},\theta}, \tag{48}$$

and analyze the cases where $\Delta F_{\mathrm{PD},\theta} > 0$.

When the non-Hermitian parameter $a < 1$, the QFI difference $\Delta\mathcal{F}_{\mathrm{PD},\theta}$ still displays periodic oscillations with a period $T_\theta = \pi/\omega$. Within the first oscillation period, the time interval where $\Delta\mathcal{F}_{\mathrm{PD},\theta} > 0$ can be derived as

$$t_\theta \in \begin{cases} (\frac{\pi}{2\omega}, \frac{\pi}{\omega}), & \Theta \in (0, \sqrt{a^2+1}-a), \\ (\frac{\pi}{2\omega}, \frac{\pi}{\omega}-\tau_1)\cup(\frac{\pi}{\omega}-\tau_2, \frac{\pi}{\omega}), & \Theta \in (\sqrt{a^2+1}-a, 1), \\ (0, -\tau_2)\cup(-\tau_1, \frac{\pi}{2\omega}), & \Theta \in (1, \sqrt{a^2+1}+a), \\ (0, \frac{\pi}{2\omega}), & \Theta \in (\sqrt{a^2+1}+a, +\infty), \end{cases} \tag{49}$$

with the definition $\Theta = \tan^2(\theta/2)$, and

$$\begin{aligned} \tau_1 &= \frac{1}{\omega}\arctan\left[\frac{a\omega(1+\Theta^2)+\omega\sqrt{4\Theta^2a^2-(1-\Theta^2)^2}}{(1+a^2)(1-\Theta^2)}\right], \\ \tau_2 &= \frac{1}{\omega}\arctan\left[\frac{a\omega(1+\Theta^2)-\omega\sqrt{4\Theta^2a^2-(1-\Theta^2)^2}}{(1+a^2)(1-\Theta^2)}\right]. \end{aligned} \tag{50}$$

For subsequent periods, the time interval can be updated by adding $k\pi/\omega$ ($k = 1, 2, \cdots$) to the upper and lower bounds.

Taking the non-Hermitian parameter $a = 0.8$ as an example, Fig. 7 (a) illustrates the evolution of $\Delta\mathcal{F}_{\mathrm{PD},\theta}$ over time for different values of parameter $\theta$. The regions where $\Delta\mathcal{F}_{\mathrm{PD},\theta} > 0$ occur periodically, and these results are consistent with the analytical results.

When the non-Hermitian parameter $a > 1$, the $\mathcal{PT}$ symmetry is broken. As time $t$ increases, the QFI difference $\Delta\mathcal{F}_{\mathrm{PD},\theta}$ tends towards a steady value, i.e.,

$$\lim_{t\to\infty}(\Delta\mathcal{F}_{\mathrm{PD},\theta}) = \frac{1}{(a+|\omega|\cos\theta)^2} - 1. \tag{51}$$

Clearly, if the non-Hermitian parameter $a$ satisfies the condition:

$$1 < a < \frac{1+\cos^2\theta}{1-\cos^2\theta}, \tag{52}$$

then $\lim_{t\to\infty}(\Delta\mathcal{F}_{\mathrm{PD},\theta}) > 0$. Taking the parameter $a = 1.01$ as an example, Fig. 7 (b) illustrates the evolution of $\Delta\mathcal{F}_{\mathrm{PD},\theta}$ over time for different values of parameter $\theta$. The regions where $\Delta\mathcal{F}_{\mathrm{PD},\theta} > 0$ are evident, demonstrating that $\mathcal{PT}$-symmetry-breaking operations enhance the QFI of $\theta$.

Additionally, we examine the variation of $\lim_{t\to\infty}(\Delta\mathcal{F}_{\mathrm{PD},\theta})$ with respect to the parameter $a$. Fig. 7 (c) shows that, for $\theta = 2\pi/3$, $\lim_{t\to\infty}(\Delta\mathcal{F}_{\mathrm{PD},\theta})$ initially increases and then decreases as $a$ increases, reaching a maximum value of $(2\sqrt{5}+1)/4$ at $a = \sqrt{5}/2$. This indicates that increasing the value of $a$ in the non-Hermitian Hamiltonian does not monotonically enhance the QFI in this case.

As demonstrated in Sec. IV B and Sec. III A, the teleported QFI is significantly enhanced by the introduction of non-Hermitian operations compared to scenarios where such operations are not employed. This enhancement can be attributed to the fact that non-Hermitian operations are typically realized through postselection measurements on the ancilla system, enabling a greater concentration of QFI within a smaller sample. Namely, the amplitude of QFI is achieved with a reduced success probability. It is important to note that when considering the entire system used to implement non-Hermitian operations, the total QFI remains unchanged [53–55].

### C. Relationship between teleportation fidelity and teleported QFI

In the scenario we are considering, the teleportation fidelity and teleported QFI display different behaviors during the evolution. However, there exists a profound relationship between the teleportation fidelity and the teleported QFI. In the case of phase-damping noise channel, by introducing a non-Hermitian operator, we derive the analytical expressions for the teleportation fidelity $F_{\mathrm{PD}}^{\mathrm{NH}}$ in Eq. (14) as well as the teleported QFI $\mathcal{F}_{\mathrm{PD},\phi}^{\mathrm{NH}}$ for the parameter $\phi$ and $\mathcal{F}_{\mathrm{PD},\theta}^{\mathrm{NH}}$ for $\theta$ in Eqs. (41, 47). Based on these expressions, we establish the following inequality

$$F_{\mathrm{PD}}^{\mathrm{NH}} + \frac{1}{2}\sin^2\theta\sqrt{\mathcal{F}_{\mathrm{PD},\theta}^{\mathrm{NH}}} - \frac{1}{2}\sin\theta\sqrt{\mathcal{F}_{\mathrm{PD},\phi}^{\mathrm{NH}}} \le 1, \tag{53}$$

where the equality holds if and only if $\mu_1 = \mu_2$, corresponding to the condition $\sin(2\omega t) = 0$. This inequality characterizes an novel trade-off relation imposed by the non-Hermitian operation on the teleportation fidelity and the teleported QFI under the influence of a phase-damping noise channel. The inequality holds regardless of whether $\mathcal{PT}$ symmetry is maintained or broken. Through this inequality, the relation between the fidelity and QFI during the teleportation process can be better understood.

Notably, in the $\mathcal{PT}$-symmetry-breaking case, as time approaches infinity, the QFI $\mathcal{F}_{\mathrm{PD},\phi}^{\mathrm{NH}}$ associated with the parameter $\phi$ tends to 0 [as derived from Eq. (41)], sim-

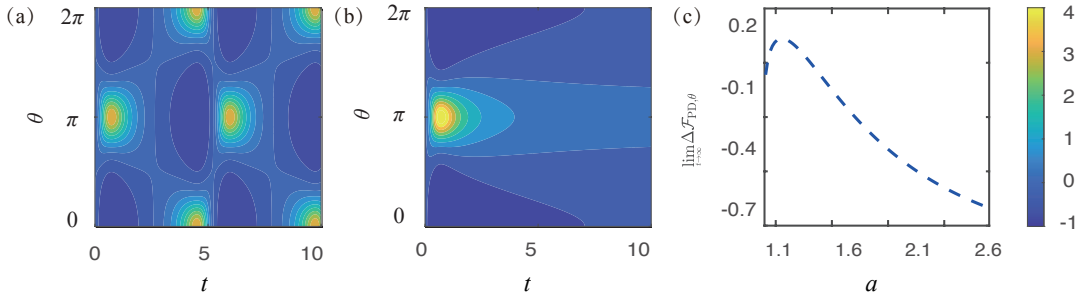


Figure 7. (a) and (b) depict the evolution of the quantum Fisher information difference $\Delta\mathcal{F}_{\mathrm{PD},\theta}$ for time $t$ and the state parameter $\theta$ under $\mathcal{PT}$-symmetric operations (with the non-Hermitian parameter $a = 0.8$) and $\mathcal{PT}$-symmetry-breaking operations (with $a = 1.01$), respectively. (c) presents $\lim_{t\to\infty}(\Delta\mathcal{F}_{\mathrm{PD},\theta})$ as a function of the non-Hermitian parameter $a$. The parameter is fixed at $\theta = 2\pi/3$.

plifying the inequality to

$$\lim_{t\to\infty} F_{\mathrm{PD}}^{\mathrm{NH}} + \frac{1}{2}\sin^2\theta\sqrt{\lim_{t\to\infty}\mathcal{F}_{\mathrm{PD},\theta}^{\mathrm{NH}}} \leq 1. \tag{54}$$

From Eqs. (53, 54), it is evident that the limited quantum resources in the quantum teleportation process impose a constraint between the teleportation fidelity and the teleported QFI. These inequality relations indicate that the variation trends of the fidelity and QFI for different parameters may not align. Notably, in the long-time limit, the steady value of fidelity may exhibit an inverse relationship with the steady value of the QFI associated with $\theta$.

## V. CONCLUSION

We investigate the effect of non-Hermitian operations on the quantum teleportation of a qubit state under the influence of phase-damping, amplitude-damping, and bit-flip channel. Our findings reveal that $\mathcal{PT}$-symmetric non-Hermitian operations induce periodic enhancement in teleportation fidelity within certain temporal domains, outperforming conventional teleportation protocol. Through analytical derivation, we identify the advantageous time intervals which are determined by the non-Hermitian parameter and channel strength. Specifically, for identical channel strengths $p_{\mathrm{PD(AD)}}$, the phase-damping channel consistently exhibits broader advantageous intervals compared to the amplitude-damping channel. However, the interval width in the phase-damping channel surpasses that of the bit-flip channel only when the channel parameter exceeds 1/2. When the non-Hermitian parameter enters the $\mathcal{PT}$-symmetry-breaking regime, the fidelity difference between the non-Hermitian and conventional approaches converges to a steady value, eliminating temporal oscillations. We derive an analytical expression for this steady fidelity, which depends on the non-Hermitian parameter, the channel parameter, and the initial state parameter.

We further examine the influence of non-Hermitian operations on the teleported quantum Fisher information (QFI), considering the coefficients $\theta$ and $\phi$ of the sender's quantum state as the parameters to be estimated. Focusing on the phase-damping noise channel, in the $\mathcal{PT}$-symmetric regime, the difference in the teleported QFI of $\phi$ between the non-Hermitian protocol and conventional protocol exhibits periodic oscillation over time. We analytically determine the advantageous time intervals and the maximum enhancement achievable. In contrast, in the $\mathcal{PT}$-symmetry-breaking regime, the QFI of $\phi$ initially increases before decaying to zero, then the QFI difference converges to a steady value. The short enhancement interval is also derived analytically. The teleported QFI of $\theta$, however, behaves differently, remaining unaffected by the noisy channel.

Moreover, we reveal the distinct behaviors between teleportation fidelity and teleported QFI. Specifically, the time interval for enhancing teleportation fidelity depends on the channel strength, whereas the time interval for improving teleported QFI is independent of the channel parameter. More importantly, we establish an inequality relationship between the teleportion fidelity and teleported QFI, offering a theoretical foundation for a deeper understanding of the quantum teleportation process. Our findings provide novel insights into the role of non-Hermitian physics in quantum information processing and lay the groundwork for enhancing the performance of quantum teleportation.

## ACKNOWLEDGMENTS

This work is supported by the Hangzhou Joint Fund of the Zhejiang Provincial Natural Science Foundation of China (Grant No. LHZSD24A050001), the National Natural Science Foundation of China (Grant Nos. 12175052, 12405026, and 12504343), the National Key Research and Development Program of China (Grant No. 2024YFA1408900), the Funds of the Natural Science Foundation of Hangzhou (Grant No. 2024SZRYBA050001), the Hangzhou Leading Youth Innovation and Entrepreneurship Team project (Grant No. TD2024005), the Zhejiang Provincial Natural Science

Foundation of China (Grant No. LQN25A040019), and the HZNU scientific research and innovation team project (TD2025003).


[1] C. H. Bennett, G. Brassard, C. Crépeau, *et al.*, Physical Review Letters **70**, 1895–1899 (1993).

[2] A. Einstein, B. Podolsky, and N. Rosen, Physical Review **47**, 777–780 (1935).

[3] D. Boschi, S. Branca, F. D. Martini, L. Hardy, and S. Popescu, Physical Review Letters **80**, 1121 (1998).

[4] X.-L. Wang, X.-D. Cai, Z.-E. Su, M.-C. Chen, D. Wu, L. Li, N.-L. Liu, C.-Y. Lu, and J.-W. Pan, Nature **518**, 516 (2015).

[5] X.-S. Ma, T. Herbst, T. Scheidl, D. Wang, S. Kropatschek, W. Naylor, B. Wittmann, A. Mech, J. Kofler, E. Anisimova, V. Makarov, T. Jennewein, R. Ursin, and A. Zeilinger, Nature **489**, 269 (2012).

[6] R. Valivarthi, M. G. Puigibert, Q. Zhou, G. H. Aguilar, V. B. Verma, F. Marsili, M. D. Shaw, S. W. Nam, D. Oblak, and W. Tittel, Nature Photonics **10**, 676 (2016).

[7] A. Karlsson and M. Bourennane, Physical Review A **58**, 4394–4400 (1998).

[8] D. Bouwmeester, J. W. Pan, K. Mattle, *et al.*, Nature **390**, 575–579 (1997).

[9] R. Horodecki, M. Horodecki, and P. Horodecki, Physics Letters A **222**, 21 (1996).

[10] C. H. Bennett and S. J. Wiesner, Physical Review Letters **69**, 2881–2884 (1992).

[11] N. Gisin, G. Ribordy, W. Tittel, *et al.*, Reviews of Modern Physics **74**, 145–195 (2002).

[12] H. J. Kimble, Nature **453**, 1023–1030 (2008).

[13] M. Gu, H. Chrzanowski, S. Assad, T. Symul, K. Modi, T. Ralph, V. Vedral, and P. Lam, Nature Physics **8**, 671 (2012).

[14] J. Lee and M. S. Kim, Physical Review Letters **84**, 4236 (2000).

[15] F. Verstraete and H. Verschelde, Physical Review Letters **90**, 097901 (2003).

[16] L. T. Knoll, C. T. Schmiegelow, and M. A. Larotonda, Physical Review A **90**, 042332 (2014).

[17] D. A. Lidar and K. B. Whaley, *Decoherence-Free Subspaces and Subsystems* (Springer Berlin Heidelberg, Berlin, Heidelberg, 2003).

[18] D. Bowman, T. L. Harte, V. Chardonnet, C. D. Groot, S. J. Denny, G. L. Goc, M. Anderson, P. Ireland, D. Cassettari, and G. D. Bruce, Optics Express **25**, 11692 (2017).

[19] M. L. Hu and L. Zhou, Physical Review A **83**, 032123 (2011).

[20] S. Oh, S. Lee, and J. Kim, Physical Review A **66**, 022316 (2002).

[21] J. Yin, Y. Cao, Y. H. Li, *et al.*, Science **356**, 1140–1144 (2017).

[22] E. Jung, M.-R. Hwang, Y.-D. Ju, M. S. Kim, S. K. Yoo, H. Kim, D. Park, J.-W. Son, S. Tamaryan, and S.-Y. Cha, Physical Review A **78**, 012312 (2008).

[23] P. W. Shor, Physical Review A **52**, R2493 (1995).

[24] C. H. Bennett, H. J. Bernstein, S. Popescu, *et al.*, Physical Review A **53**, 2046 (1996).

[25] B. M. Terhal, Reviews of Modern Physics **87**, 307 (2015).

[26] A. G. Fowler, M. Mariantoni, J. M. Martinis, *et al.*, Physical Review A **86**, 032324 (2012).

[27] E. T. Campbell, B. M. Terhal, and C. Vuillot, Nature **549**, 172–179 (2017).

[28] N. Hatano and D. R. Nelson, Physical Review Letters **77**, 570 (1996).

[29] N. Moiseyev, *Non-Hermitian Quantum Mechanics* (Cambridge University Press, Cambridge, 2011).

[30] S.-Y. Zang, M.-F. Fang, and L. Xu, Quantum Information Processing **16**, 234 (2017).

[31] W. Ding, X. Wang, and S. Chen, Physical Review Letters **131**, 160801 (2023).

[32] X. Yu, X. Zhao, L. Li, X.-M. Hu, X. Duan, H. Yuan, and C. Zhang, Science Advances **10**, eadk7616 (2024).

[33] X. Yu and C. Zhang, Physical Review A **108**, 022215 (2023).

[34] C. M. Bender and S. Boettcher, Physical Review Letters **80**, 5243 (1998).

[35] W.-Y. Li and L. Ye, International Journal of Theoretical Physics **60**, 2878 (2021).

[36] F. Roccati, S. Lorenzo, G. Palma, G. Landi, M. Brunelli, and F. Ciccarello, Quantum Science and Technology **6**, 025005 (2021).

[37] J. Ramya Parkavi, R. Muthuganesan, V. Chandrasekar, and M. Lakshmanan, Physica A: Statistical Mechanics and its Applications **615**, 128586 (2023).

[38] L. Xiao, K. Wang, X. Zhan, Z. Bian, K. Kawabata, M. Ueda, W. Yi, and P. Xue, Physical Review Letters **123**, 230401 (2019).

[39] K. Kawabata, Y. Ashida, and M. Ueda, Physical Review Letters **119**, 190401 (2017).

[40] M. M. Wilde, *Quantum Information Theory* (Cambridge University Press, 2013) comprehensive introduction to the theory of quantum information.

[41] M. A. Nielsen and I. L. Chuang, *Quantum Computation and Quantum Information* (Cambridge University Press, 2010) standard textbook on quantum information theory.

[42] V. Giovannetti and R. Fazio, Physical Review A **71**, 032314 (2005).

[43] C. W. Helstrom, *Quantum Detection and Estimation Theory* (Academic Press, 1976) fundamental work on quantum estimation theory.

[44] A. S. Holevo, *Probabilistic and Statistical Aspects of Quantum Theory* (Springer Science & Business Media, 2011) covers statistical aspects of quantum theory.

[45] H.-M. Yu and J. Liu, Fundamental Research (2025), 10.1016/j.fmre.2025.02.020.

[46] J. Liu and H. Yuan, Physical Review A **96**, 042114 (2017).

[47] J. Liu, X. Jing, and X. Wang, Scientific Reports **5**, 8565 (2015).

[48] J. Liu, H. Xiong, F. Song, and X. Wang, Physica A: Statistical Mechanics and its Applications **410**, 167 (2014).

[49] P.-F. Wei, Q. Luo, H.-Q.-C. Wang, S.-J. Xiong, B. Liu, and Z. Sun, Frontiers of Physics **19**, 21201 (2024).

[50] M. Zhang, H. Yu, and J. Liu, npj Quantum Information **9**, 97 (2023).

[51] Z. Sun, J. Ma, X.-M. Lu, and X. G. Wang, Physical Review A **82**, 022306 (2010).
[52] W. Zhong, Z. Sun, J. Ma, X. Wang, and F. Nori, Physical Review A **87**, 022337 (2013).
[53] Y. Chu, Y. Liu, H. Liu, and J. Cai, Physical Review Letters **124**, 020501 (2020).
[54] L. Zhang, A. Datta, and I. Walmsley, Physical Review Letters **114**, 210801 (2015).
[55] N. Lupu-Gladstein, Y. B. Yilmaz, D. R. M. Arvidsson-Shukur, A. Brodutch, A. O. T. Pang, A. M. Steinberg, and N. Y. Halpern, Physical Review Letters **128**, 220504 (2022).